



HAL
open science

Prospects for a modular Inductive Adder pulse generator for $300\mu\text{s}$ and $90\mu\text{s}$ pulse widths of HEP accelerators dump systems

J Rodziewicz

► To cite this version:

J Rodziewicz. Prospects for a modular Inductive Adder pulse generator for $300\mu\text{s}$ and $90\mu\text{s}$ pulse widths of HEP accelerators dump systems. [Research Report] CERN. 2020. hal-02891469v1

HAL Id: hal-02891469

<https://hal.science/hal-02891469v1>

Submitted on 6 Jul 2020 (v1), last revised 7 Jul 2020 (v2)

HAL is a multi-disciplinary open access archive for the deposit and dissemination of scientific research documents, whether they are published or not. The documents may come from teaching and research institutions in France or abroad, or from public or private research centers.

L'archive ouverte pluridisciplinaire **HAL**, est destinée au dépôt et à la diffusion de documents scientifiques de niveau recherche, publiés ou non, émanant des établissements d'enseignement et de recherche français ou étrangers, des laboratoires publics ou privés.

Prospects for a modular Inductive Adder pulse generator for $300\mu\text{s}$ and $90\mu\text{s}$ pulse widths of HEP accelerators dump systems

J. Rodziejewicz

janusz_rodziejewicz@yahoo.pl

CERN TE-ABT, Geneva, Switzerland

Abstract

This document describes the operation principle and design steps of a modular Inductive Adder (IA) pulse generator delivering relatively long, high-current pulses. Two case studies will be employed, Future Circular Collider - like design (FCC), and Large Hadron Collider - like design (LHC). AC (Alternative Current) IA topology brings the high modularity into the generator design, aiming a moderate high voltage stress of power components (mainly switches) and mitigation of consequences due to critical failure modes of individual semiconductors, such as missing or erratics.

1 Principle

1.1 Oscillation rectifying

Thanks to the rectifying stage and a high-frequency alternative flux in the IA magnetic core, the device can generate long, high current pulses to the RL load. Multiple paralleled branches allow to add individual currents into one high, magnet current. Multiple in vertical plane stages increase the overall, IA output voltage. Therefore, lower rating semiconductor switch can be considered in each of modular cell.

Typical IA previously introduced in number of pulsed power systems delivers the pulses in ns or few μs range. Most often, due to requirement on ns-short rise times, care is taken to the IA impedance, in considered dumping system the rise-time requirements are much more relaxed, and parallel branches are sharing the overall, source impedance, therefore less attention is paid to the geometry aspects. Other benefits of of discussed typologies will be highlighted across the document. The rectifying principle within the AC IA topology can be represented in figure 1.

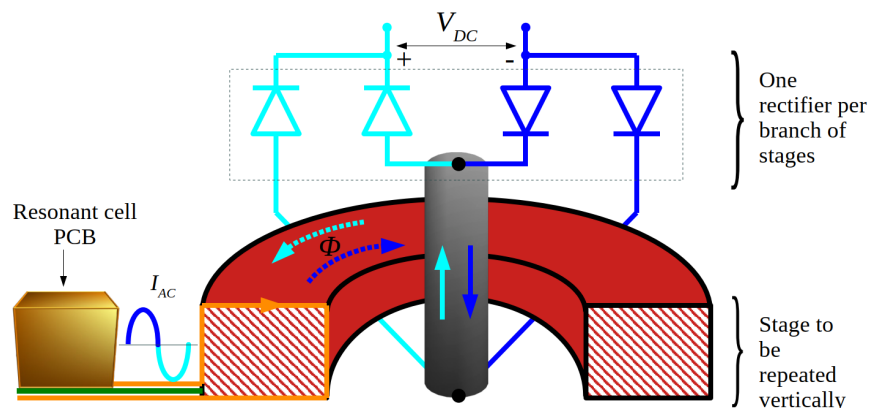


Figure 1: Principle of an AC Inductive Adder with a diode bridge stage. Here, the current flows through the load connected between the voltage output terminals.

Multiple in horizontal plane branches (N_{br} - the number of branches) are formed by multiple in vertical plane stages (N_{stg} - the number of stages).

2 A discharge switch-based architecture

The alternative flux in the core will forced by the alternative, discharge current of multiple primaries - series LC circuits. The discharge of the each cell primaries is triggered by the closure of one, common switch, which will remain closed over the whole pulse length. The arrangement of cell elements is visualised in figure below (figure 2). The schematic of the ORC is depicted in figure 3.

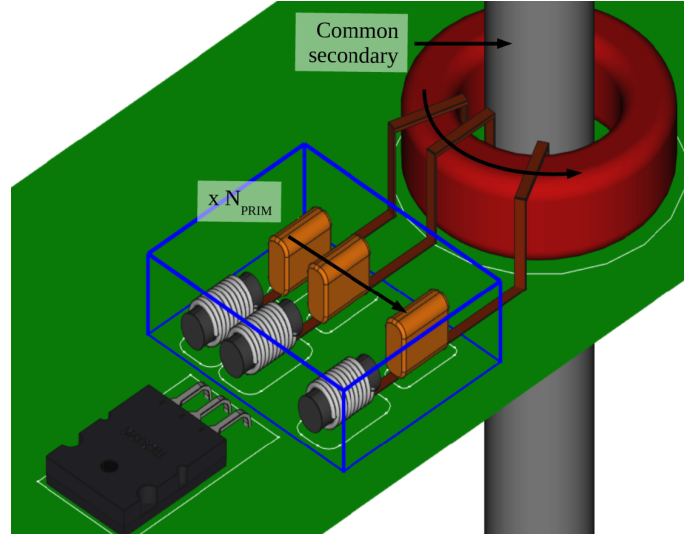


Figure 2: Oscillating Resonant Cell (ORC) view, multiple primaries are coupled independently to the magnetic core. N_{PRIM} is the number of primaries of each cell.

2.1 Control through hysteresis

The principle of power flow control is ensured by the magnetic core hysteresis (see figure 4). The power flow to the load will take place over the period θ_1 (see figure 5) for both positive and negative half-sine oscillations of the cell current (diode bridge rectification). The time interval θ_0 is required for the polarity reversal of the cell current.

2.2 Generator considerations

The requirements of the output current pulse in terms of rise time and pules length doesn't allow to use an optimal, single-type cell within considered generator. Therefore so called principal circuit (fast rise time) and compensation circuit (the pulse length requirement) will be used. The natural frequency of the principal circuit will be much higher than of the compensation circuit, respectively $\omega_P \gg \omega_C$.

In order to avoid a potential cross-coupling, the principal and compensation circuits will be separated from each other, sitting at separate branches with independent diode bridges.

2.3 Typical waveforms

2.3.1 Rise time

The role of the principal circuit is to ensure the magnet current rise time to its nominal value I_m within the specified rise time t_R . To achieve this, the initial energy, initially stored in the electric field of the

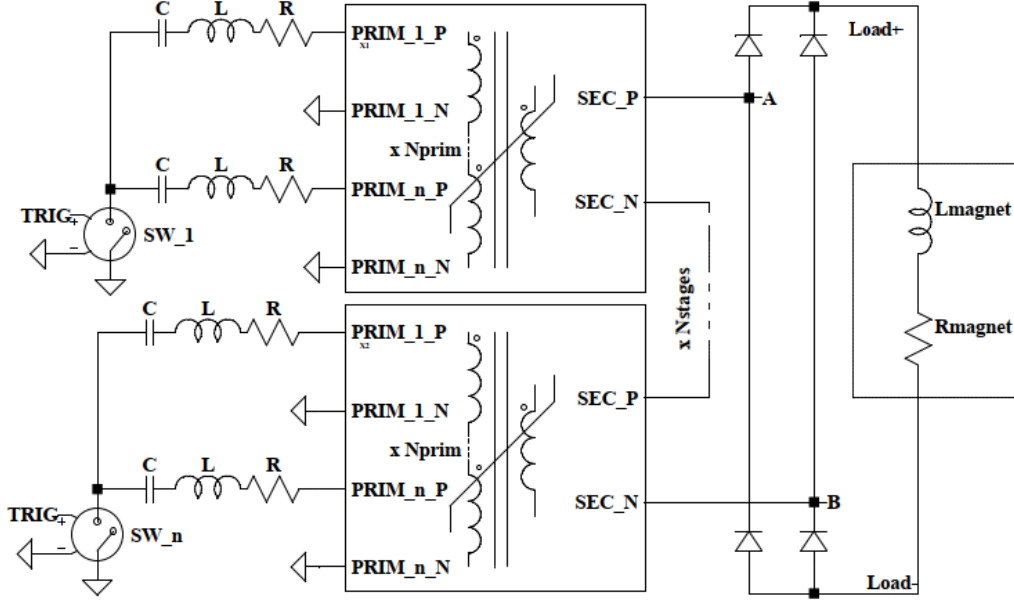


Figure 3: The secondaries of each cell are connected in series, making a branch. Cell is comprised of multiple series LC circuits, each circuit has an independent, one-turn primary.

capacitors has to be higher than the energy of the magnetic field in the magnet coil carrying the nominal I_m . The discharge will be damped by a non-zero stray resistance of cells and magnet load.

As mentioned previously, in figure 5 we distinguish the conduction period θ_1 where combined branches current equals load current and so called short period θ_0 , where the core is saturated and the cell current makes a half-sine of the ω_P (determined by principal cell parameters $C_P L_P R_\sigma$) before it changes the sign:

$$\theta_0 = \pi \sqrt{C_P L_P} \quad (1)$$

After the conduction interval, once the maximal flux is reached in the core, the flux density B more or less levels off, voltage across the output of the generator drops nearly to zero, the magnet current freewheels through the diode bridge. As depicted in figure 5, the conduction period length θ_1 will be determined by the voltage seen by the primary and principal core cross-section. As the voltage amplitude V_{PRIM} over considered period will be varying in time, averaging over t_R will be applied:

$$\theta_{1av} = \frac{A_C \Delta B}{V_{PRIMav}} \quad (2)$$

The magnetic material that will be assumed in this study is noncrystalline - VITROPERM 500F, for which the $\Delta B = 2 \cdot 1.2 T$, this material exhibits also less losses than conventional ferrite powder materials, around 80 mWg^{-1} at 100 kHz.

The averaged model requires an additional parameter D , which is the total conduction time over the rise time:

$$D = \frac{\theta_{1av}}{\theta_{1av} + \theta_0} \quad (3)$$

The optimal, averaged over the t_R , total secondary voltage V_{avr} required to ramp the current up to I_m will be defined by the inductive rise time limit (see equation 4). The voltage amplitude attenuation is

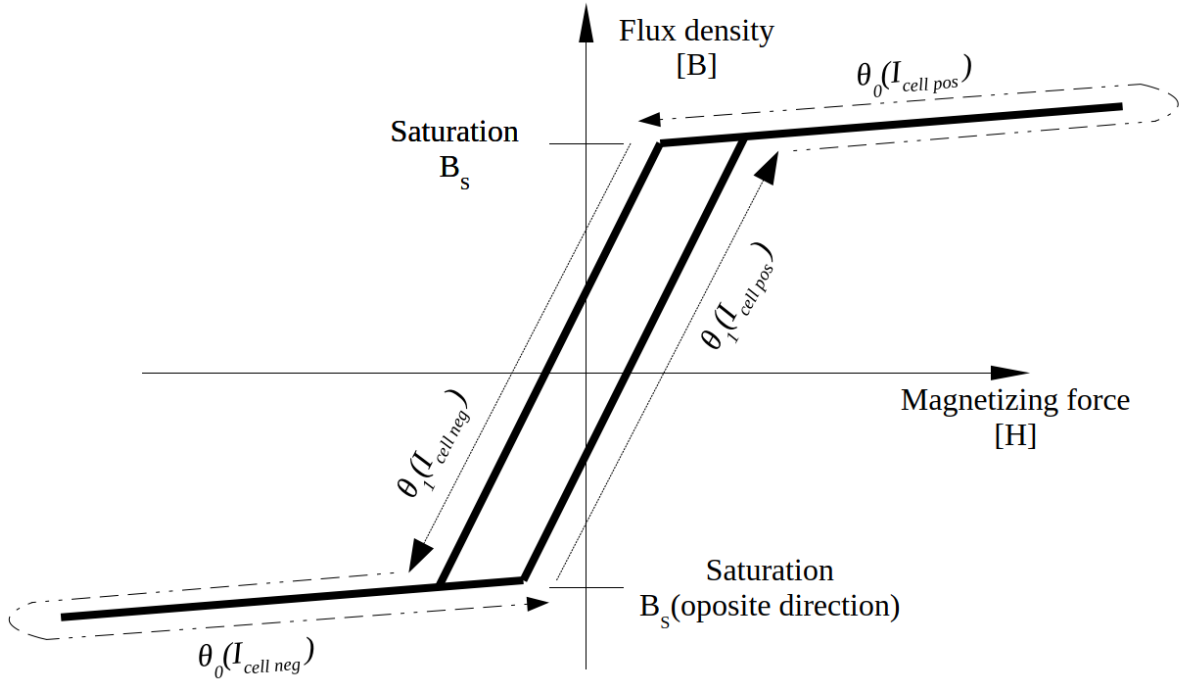


Figure 4: Hysteresis and characteristic times θ_1 and θ_0 .

α_{avg} (see figure 5):

$$\begin{cases} V_{avg} = \frac{L_1 I_m}{t_R} \\ V_{avg} = V_{init} \left[1 - \frac{e^{-\alpha_{avg} t_R}}{\alpha_{avg}} \right] \frac{D}{t_R} \end{cases} \quad (4)$$

where L_1 is the total conduction inductance, same for resistance R_1 :

$$L_1 = \frac{L_P N_{stg}}{N_{br} N_{PRIM}} + L_{magnet} \quad (5)$$

$$R_1 = \frac{R_\sigma N_{stg}}{N_{br} N_{PRIM}} + R_{magnet} \quad (6)$$

in the same way we define the equivalent capacitance of the conduction circuit:

$$C_{eq} = \frac{C_P N_{br} N_{PRIM}}{N_{stg}} \quad (7)$$

The instantaneous, peak voltage of the capacitor just before the t_R should be sufficient to deliver the nominal current I_m to the load. As the $\omega > \alpha$ the circuit will be under-damped case:

$$V_{init} e^{-\alpha_{avg}(t_R - \frac{\pi}{2\omega_1})} \frac{1}{L_1 \omega_1} = I_m \quad (8)$$

where, ω_1 is the natural frequency associated with the conduction circuit:

$$\omega_1 = \frac{1}{\sqrt{L_1 C_{eq}}} \quad (9)$$

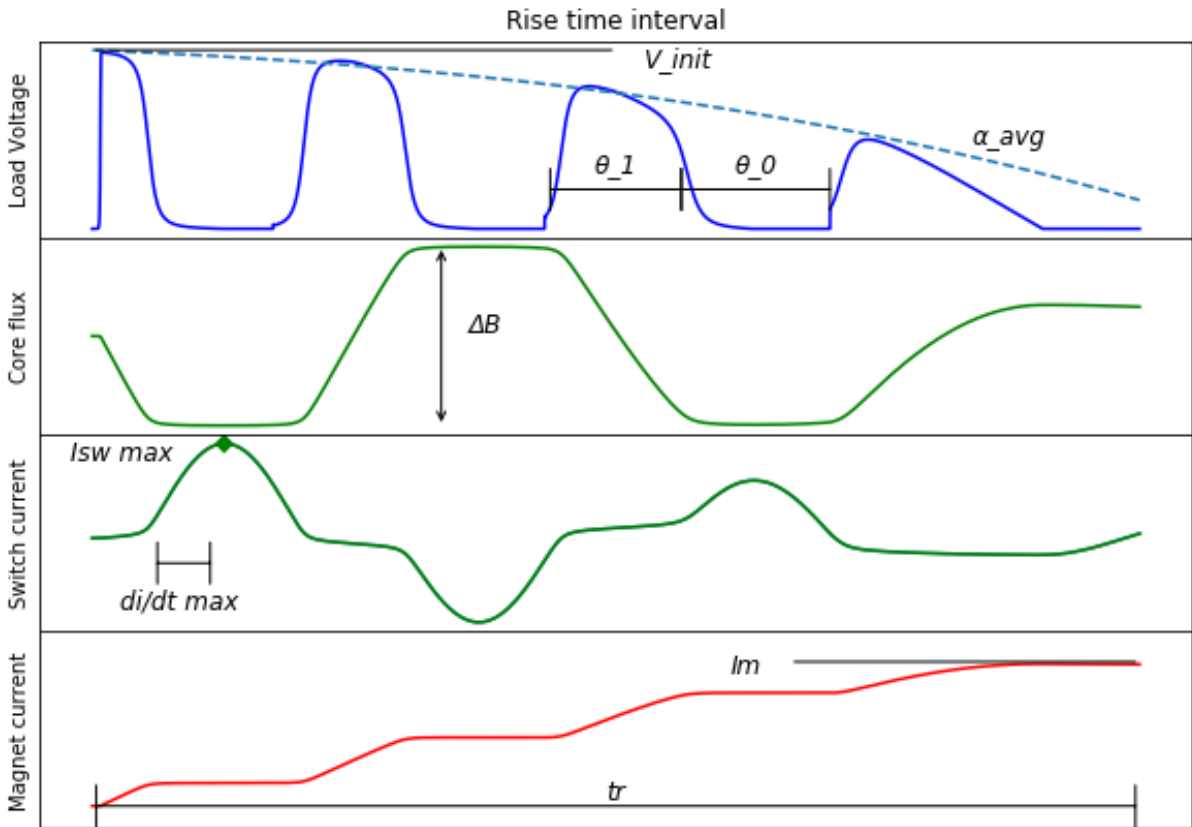


Figure 5: Typical waveforms associated with the rise time interval.

2.3.2 Pulse flattop

The pulse flattop will be ensured by the compensation circuit ($L_C C_C R_\sigma$), in order to optimise it, we consider the initial current in the magnet coil nominal I_m (figure 6 gives the associated waveforms). Over the conduction time θ_1 the current is being ramped-up to $d \cdot I_m$. As previously for the principal circuit, we distinguish ω_1 associated with the conduction circuit and ω_C associated with each individual primary:

$$\omega_C = \frac{1}{\sqrt{L_C C_C}} \quad (10)$$

Here, the conduction time is assumed to vary only slightly over the flattop:

$$\theta_1 = \frac{L_{cond} 2d}{V_{PRIM} N_{stg}/I_m - R_{cond}} \quad (11)$$

The requirement on the output current ripple will define the time θ_0 required for the cell compensation current I_c (switch current) to change polarity and reverse the trend of the magnet current at $I_m(1-d)$ instant (see figure 6).

$$\omega_c = -\frac{\pi}{\tau \log\left(\frac{1-d}{d+1}\right)} \quad (12)$$

where,

$$\tau = \frac{L_{magnet}}{R_{magnet}} \quad (13)$$

θ_0 defines the half-period of the proper, cell natural frequency ω_c , as per (1).

In order to maintain the ripple within the specifications over the flattop length, the dumping of the oscillating circuit should be kept low. As the discharge current of the capacitor of each cell leaps between the conduction circuit (θ_1) and cell circuit (θ_0), the average attenuation α_{avg} will be the arithmetic average of α_C ($C_C L_C$) and α_1 ($C_{eq} L_1$ of compensation):

$$\alpha_{avg} = \frac{\theta_1 \alpha_1 + \frac{\pi}{\omega_c} \alpha_c}{\theta_1 + \pi/\omega_c} \quad (14)$$

where,

$$\alpha_c = \frac{R_\sigma}{2L_c} \quad (15)$$

$$\alpha_1 = \frac{R_1}{2L_1} \quad (16)$$

Now, the peak voltage of cell capacitors at pulse end t_{end} can be described as:

$$V_0 = V_{init} e^{-\alpha_{avg} t_{end}} \quad (17)$$

If, considered oscillations are satisfying the conditions of the under-damped oscillating circuits $\omega > \alpha$, we write the condition (at the primary) for the peak current at the end of the flattop:

$$I_m(1-d) < \frac{V_0}{L_1 \omega_1} \quad (18)$$

In order to define the optimal capacitor C_C a proper energy balance has to be ensured, meaning that after t_{end} (flattop length) the total energy E_{end} stored in C_{eq} will be sufficient to feed the $I_m \cdot (1-d)$ current amplitude into the load.

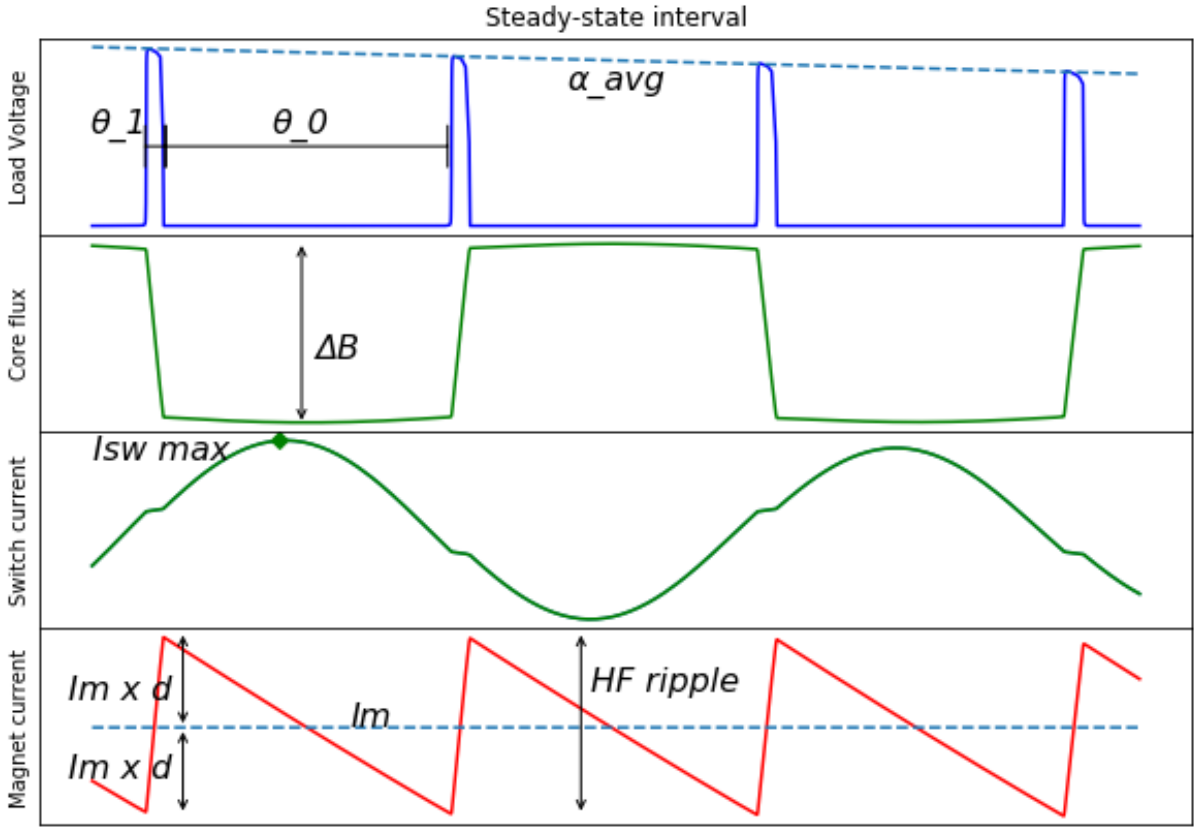


Figure 6: Typical waveforms associated with the flattop (quasi steady-state) interval.

$$req E_{end} = 0.5 C_{eq} V_0^2 \quad (19)$$

The initial energy of C_{eq} will be E_{init} , the energy loss over the t_{end} flattop will be: ΔE_{Rm} - dissipated into the magnet resistance and $\Delta E_{R\sigma}$ - dissipated into stray resistances of all cells and heat loss in magnetic cores.

The compensation circuit dimensioning assumes the initial magnet current equal to I_m , at t_{end} this current should be still flowing through the magnet, therefore, the related with it coil energy will be omitted in the energy balance.

$$E_{init} = 0.5 C_C V_{cell}^2 N_{br} N_{stg} N_{PRIM} \quad (20)$$

$$\Delta E_{R\sigma} = I_{cRMS}^2 R_{\sigma} N_{stg} N_{br} N_{PRIM} t_{end} \quad (21)$$

where, I_{cRMS} is the RMS current of the individual cell over the t_{end} flattop.

$$\Delta E_{Rm} = I_m^2 R_m t_{end} \quad (22)$$

According to above definitions we can rewrite the energy balance condition:

$$E_{init} > req E_{end} + \Delta E_{Rm} + \Delta E_{R\sigma} \quad (23)$$

2.3.3 Cross-coupled trans-conductances transformer model

In discharge switch-based architecture, a model for saturation characteristics of each stage core is required. In simulations that will be presented later in this document we use a freeware SPICE software *LTspice*.

In the *LTspice*, typical K-statements don't work with the non-linear inductor since the Chan model (saturable inductor) assumes the field is uniform in the air and core and the field won't be uniform if $K \neq 1$. Therefore, the model transformer will share the input of an ideal transformer with an inductor that saturates. The inductor is modeled with the core property parameters: H_c - Coercive Force, B_r - Remnant Flux Density, B_s - Saturation Flux Density and the mechanical dimensions of the core A_c - cross-section area, L_m - Magnetic Length

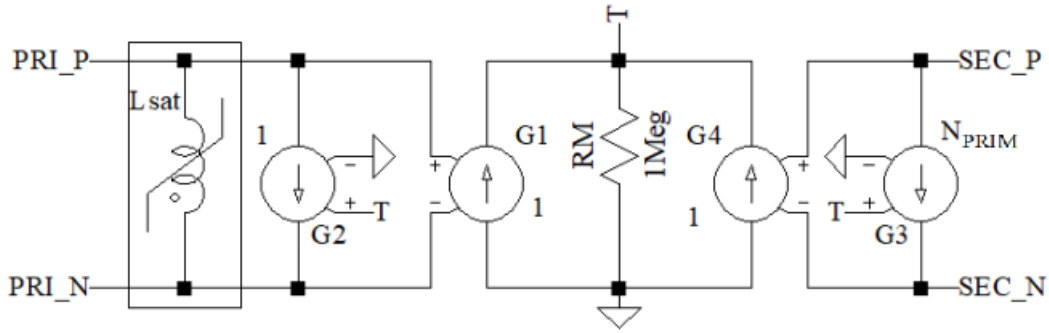


Figure 7: Ideal, cross-coupled trans-conductance transformer, saturable characteristics will be ensured by the Chan-model inductor L_{sat} . Parameter N_{PRIM} will model multiple primary winding (*LTspice*).

All winding are single-turn, the voltage controlled current sources (from $G1$ to $G4$) dependencies can be described as for ideal, multi-primary transformer:

$$\begin{cases} \frac{I_P}{I_S} = \frac{1}{N_{PRIM}} \\ \frac{V_P}{V_S} = 1 \end{cases} \quad (24)$$

3 Design examples

3.1 A 300 μ s pulse generator

As a study example, the basic parameters, similar to those of FCC beam dump, kicker generator will be employed. Many non-critical elements of the load were neglected or simplified, also the load resistance is a simple measurement-based estimation. The table 1 gives the assumed for the purpose of the study parameters:

Table 1: Assumed for the purpose of the study, FCC kicker requirements.

System parameter	Symbol	Value
Magnet inductance ^a	L_{magnet}	0.7 μ H
Magnet resistance ^a	R_{magnet}	18 m Ω
100 prc. kick current	I_m	3.3 kA
Pulse length	t_{end}	300 μ s
Current rise time	t_R	1 μ s
Peak power ^b	P_{peak}	3.8 MW

^a Altogether with cables.

^b From the energy required over the t_R .

3.1.1 FCC kicker generator principal circuit

Following the description of dependencies in 2.3.1 a *PythonSymPy* open source computer algebra system has been used to find the optimal cell capacitor C_P . Following the solution for ω_P , the inductance L_P and N_{PRIM} could be selected in order to meet the maximum allowable switch current (see figure 5).

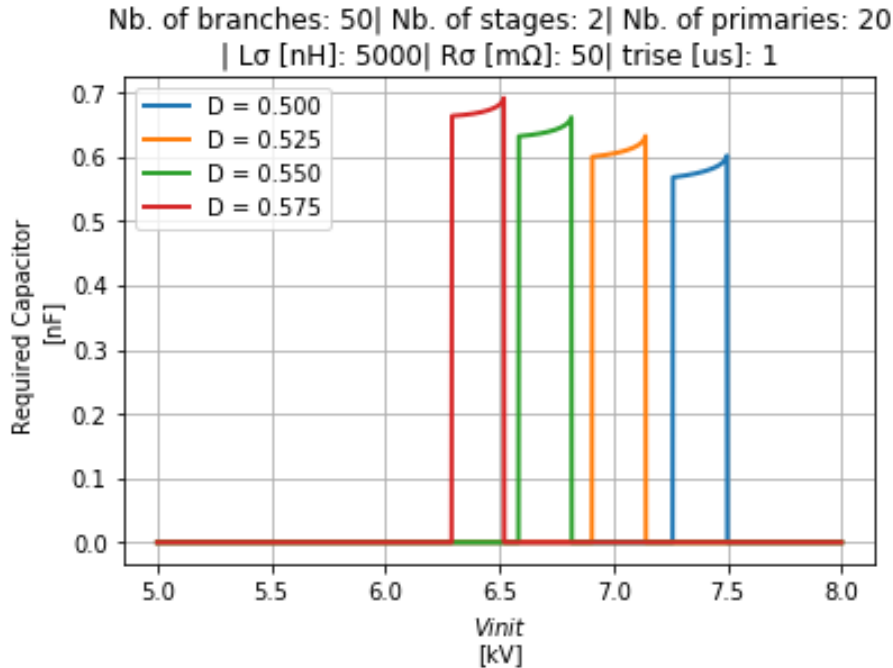


Figure 8: Solutions for cell capacitor as a function of the total generator initial voltage and D-factor (*PythonSymPy*).

In characteristics figure 8, the number of branches and stages is predefined basing on the switch technology to be used, we target HV IGBT. Bigger D will result in bigger core according to (2), therefore we select the $D = 0.525$ and 7 kV as a good compromise. In assumed structure, the optimal value of cell capacitor have been found to be:

$$C_P = 0.61nF \quad (25)$$

Resulting requirement for the magnetic core cross-section is:

$$A_P = 1.02cm^2 \quad (26)$$

3.1.2 FCC kicker generator compensation circuit

According to the description given in 2.3.3 of this document, the compensation circuit natural frequency ω_C will be set by the ripple requirements (12), also (2) links the core cross section and applied voltage-time product. A basic characteristic can be traced assuming same as in principal circuit initial voltage of 7 kV:

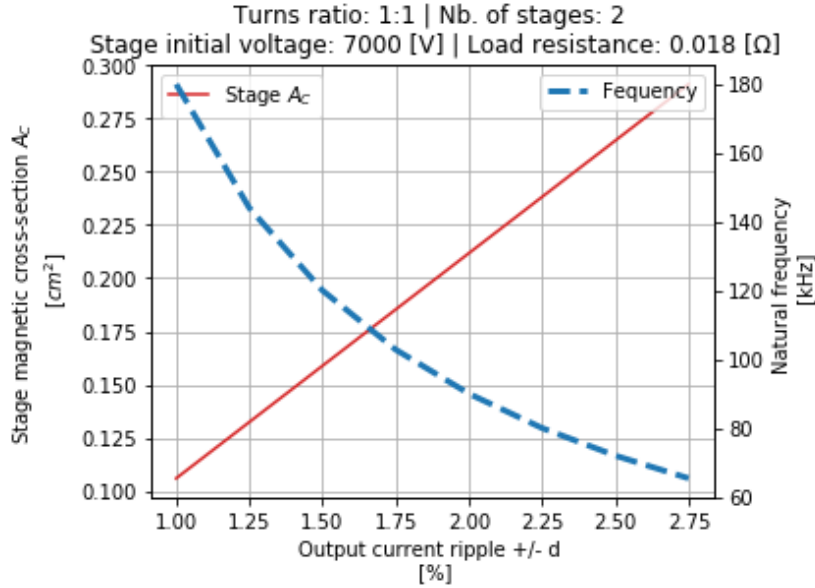


Figure 9: Basic characteristics of the FCC generator compensation circuit.

From figure 9 it appear, that lower ripple comes along with a smaller core, naturally such operation point will require a small L_C or big number of primaries N_{PRIM} leading to an important switch peak current over the short period (see 6). To overcome these limitations the number of branches N_{br} is very high, thanks to this the d as low as 2 % is expected (HF ripple 4% see definition figure 6). As per (2) and (11), resulting requirement for the core cross-section will be:

$$A_C = 0.22cm^2 \quad (27)$$

Once again we'll use the *PythonSymPy* to trace the energy balance (see 2.3.3) in function of cell capacitor C_C , see figure 10.

Obtained value of the capacitor guaranteeing a correct balance in this configuration will be:

$$C_C = 1.12nF \quad (28)$$

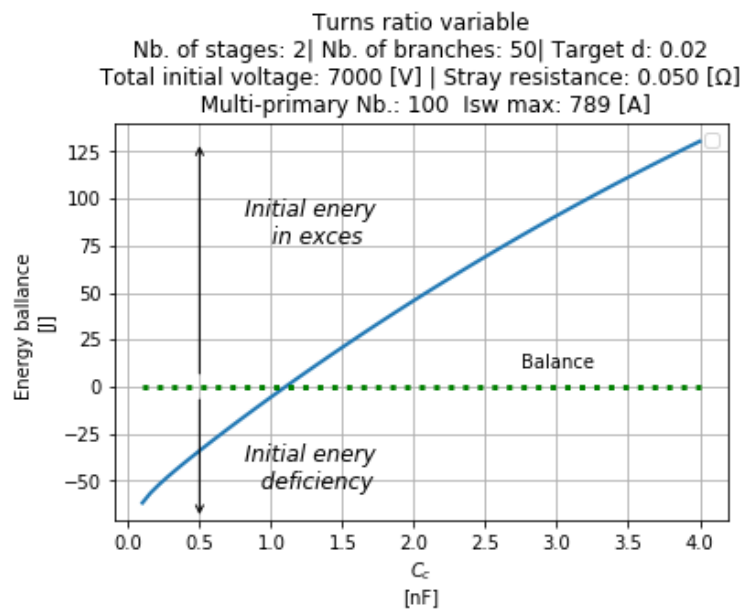


Figure 10: Compensation circuit energy balance.

3.1.3 SPICE Simulation of FCC-like generator

Table 2 lists the parameters slightly adjusted due to differences between the analytical and SPICE model. The differences can be explained by: presence of leakage resistances in SPICE model; precision of exponential functions interpolations in *Python.Sympy* formulas; for the first pulse, the flux density swing $\Delta B = 1.1T$ instead of $2.2T$ as the core is unbiased; principal and compensation circuits were dimensioned separately, in fact compensation current adds a bit to the principal, therefore N_{PRIM} had to be reduced in order to avoid the magnet current overshoot.

Table 2: FCC generator SPICE simulation parameters entries.

Parameter	Symbol	Value
Number of branches	N_{br}	50
Number of stages	N_{stg}	2
One stage voltage	V_{init}/N_{stg}	7 kV/ N_{stg}
Principal cell parameters		
Cell capacitor	C_P	0.65 nF
Cell inductor	L_P	5 μ H
Cell stray resistance	R_σ	50 m Ω
Number primaries	N_{PRIM}	10
Core cross section	A_P	1.7 cm ²
Compensation cell parameters		
Cell capacitor	C_C	1.12 nF
Cell inductor	L_C	240 μ H
Cell stray resistance	R_σ	50 m Ω
Number primaries	N_{PRIM}	120
Core cross section	A_C	0.26 cm ²

3.1.3.1 FCC generator SPICE simulation of nominal waveform

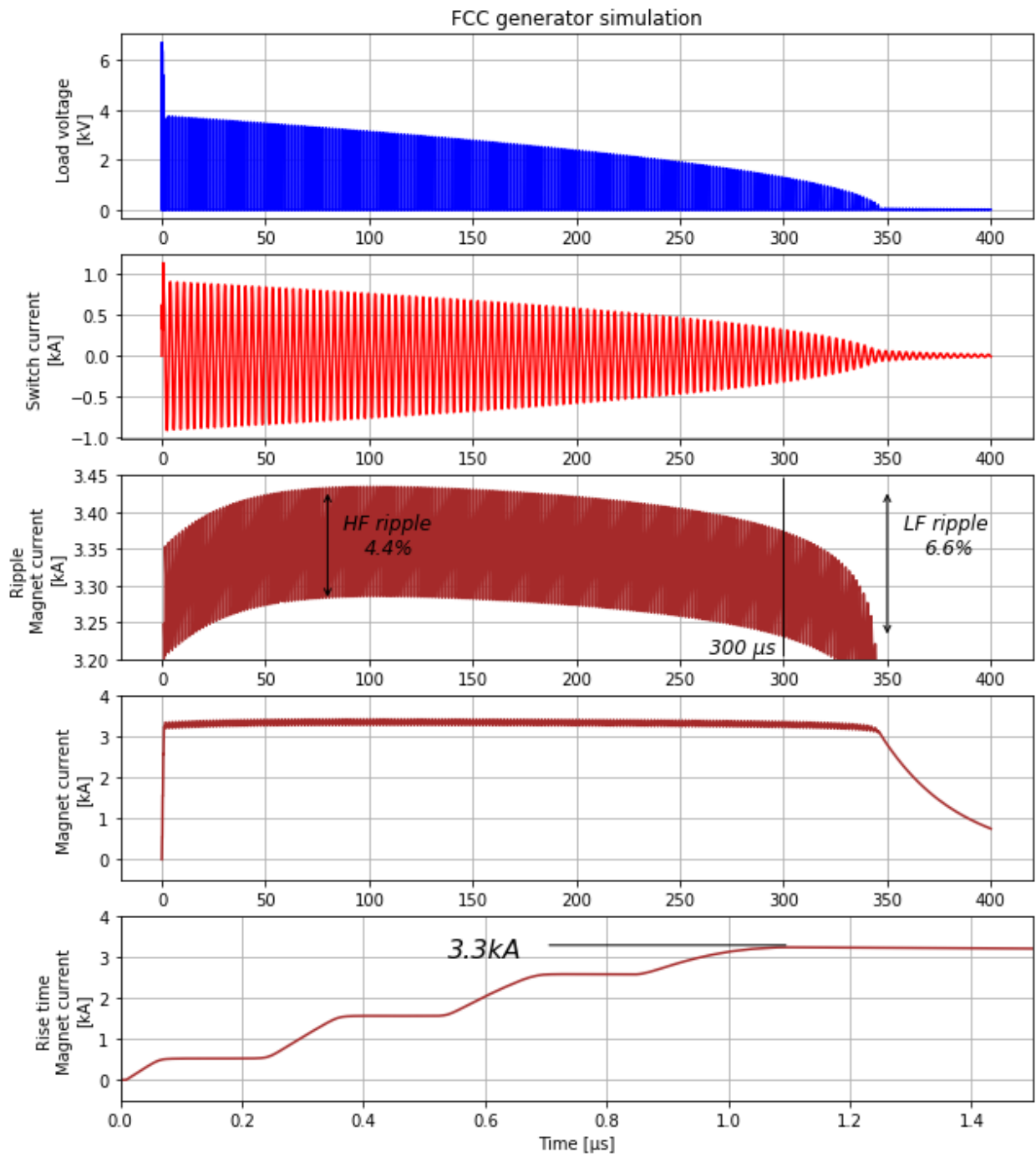


Figure 11: FCC generator simulation of the nominal waveform.

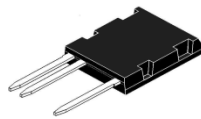
3.1.3.2 FCC generator, basic semiconductor switch considerations

Collected waveforms indicate HV IGBT as the most suitable technology regarding configuration Tab. 2.

Table 3: FCC generator switch, basic requirements.

Parameter	Symbol	Value
Collector Emitter Voltage	V_{CES}	$> 3.5 \text{ kV}$
Continuous DC collector current (at 25°C)	I_{C25}	$> 10 \text{ A}$
Maximum pulsed collector current (0.3ms)	I_{CM}	$> 1.1 \text{ kA}$
Saturation voltage	$V_{CE(sat)}$	$< 5 \text{ V}$
Maximum non-repetitive rise rate	di/dt_{max}	$> 7 \text{ kA}/\mu\text{s}$

High Voltage
XPT™ IGBT
ISOPLUS iS-Pak™



IXYL60N450

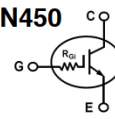


Figure 12: Potentially compatible semiconductor switch from IXYS, model IXYL60N450.

3.1.3.3 FCC generator SPICE simulation of one switch spontaneous trigger

The modular approach will allow to limit the consequences of possible cell spontaneous trigger. Simulation will predict the current and peak energy in the magnet due to this failure mode:

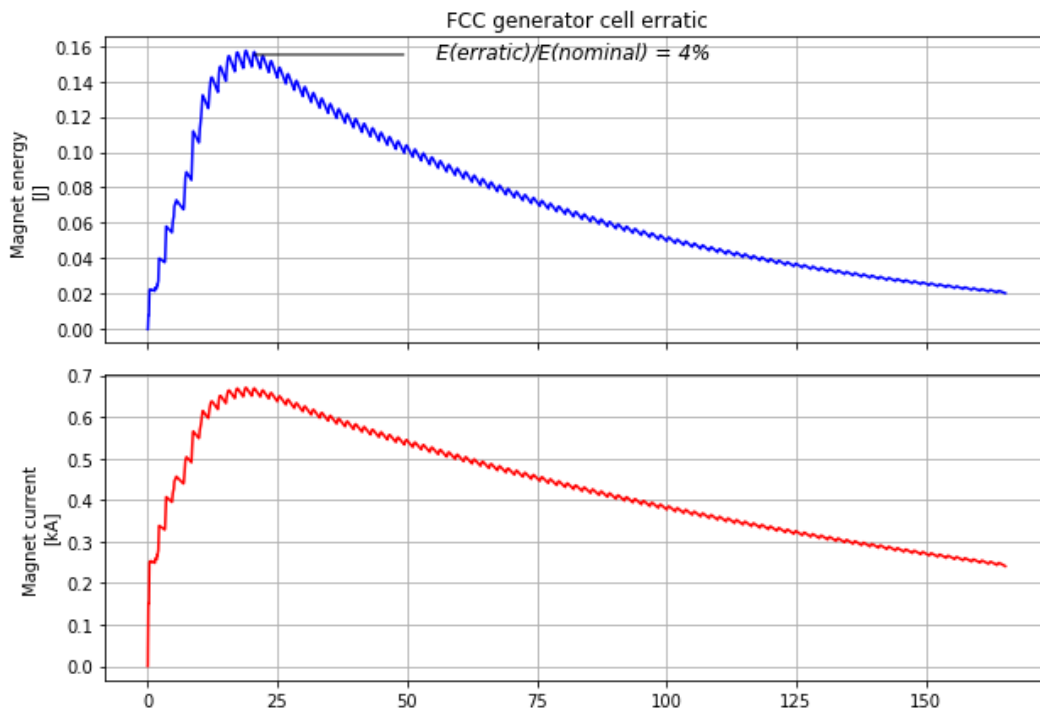


Figure 13: FCC generator simulation of one cell spontaneous trigger.

3.1.4 FCC generator assembly considerations

For the purpose of assembly considerations the nanocrystalline VITROPERM cores with epoxy resin coating were selected. Principal core of each cell will be obtained with 4 stacked L2040-W624 cores. Compensation core will be obtained using one single L2030-W676 core. The rectifiers of each branch are not represented in figure 14.

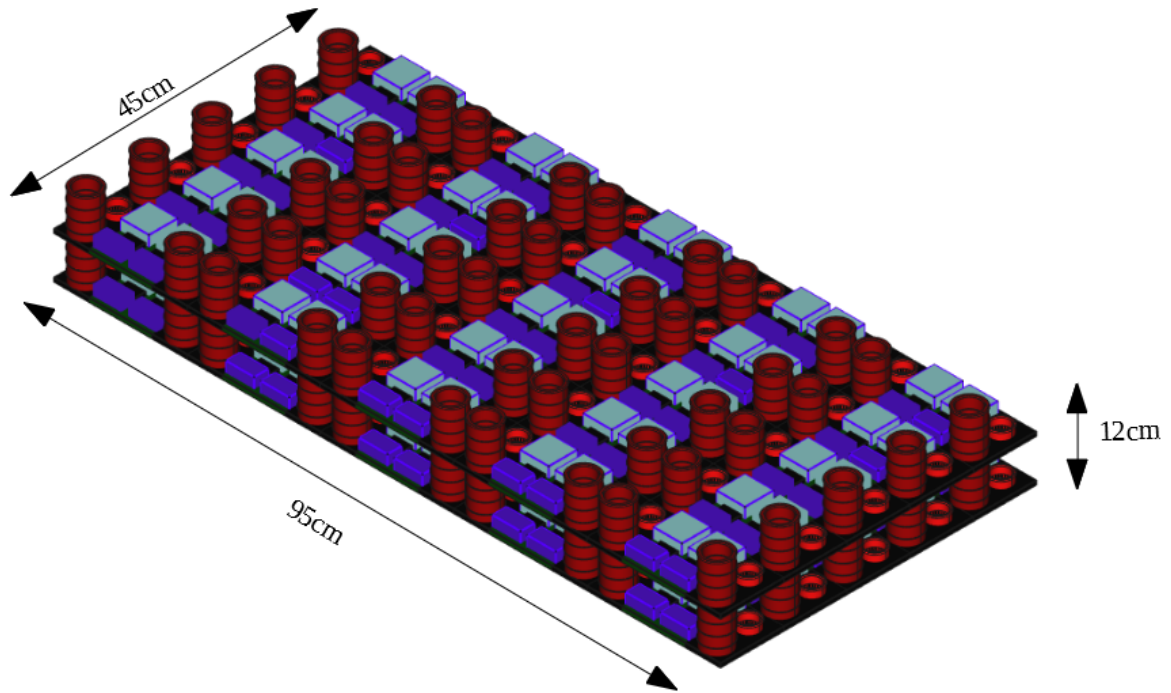


Figure 14: FCC generator assembly view (*FreeCAD*).

3.2 A 90 μ s pulse generator

The same dimensioning method will be applied for an example kicker generator, similar to this, currently operating in the LHC beam dump. Many non-critical elements of the load were neglected or simplified, also the load resistance is a simple measurement-based estimation. The table 4 gives the assumed for the purpose of the study parameters:

Table 4: Assumed for the purpose of the study, LHC kicker requirements.

System parameter	Symbol	Value
Magnet inductance ^a	L_{magnet}	2.5 μ H
Magnet resistance ^a	R_{magnet}	60 m Ω
100 prc. kick current	I_m	20 kA
Pulse length	t_{end}	90 μ s
Current rise time	t_R	3 μ s
Peak power ^b	P_{peak}	167 MW

^a Altogether with cables.

^b From the energy required over the t_R .

3.2.1 LHC kicker generator principal circuit

Following the description of dependencies in 2.3.1 a *PythonSymPy* open source computer algebra system has been used to find the optimal cell capacitor C_P . According the solution for ω_P , the inductance L_P and N_{PRIM} could be selected in order to meet the maximum allowable switch current (see figure 5). The capacitor can be chosen for a given voltage (all stages) and D factor:

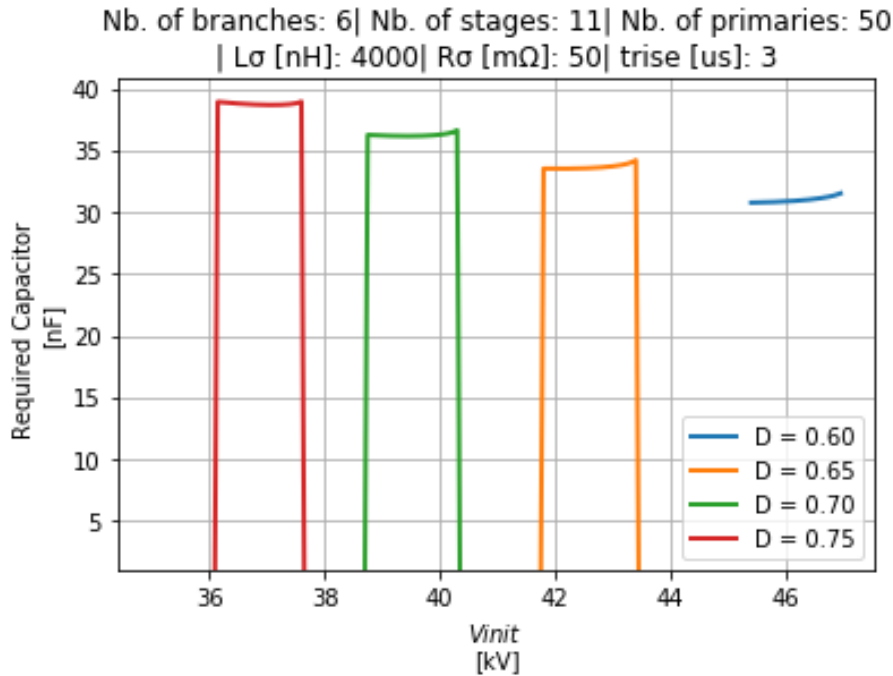


Figure 15: Solutions for cell capacitor as a function of the total generator initial voltage and D-factor (*PythonSymPy*).

The number of branches and stages is predefined basing on the switch technology to be used, we target the Fast High Current Thyristor (FHCT). Bigger D will result in bigger core according to (2), therefore we select the $D = 0.7$ and 39 kV as a good compromise. Also lower voltages will result in a higher current following the peak power requirement. In assumed structure, the optimal value of cell capacitor have been found to be:

$$C_P = 36.2nF \quad (29)$$

Resulting requirement for the magnetic core cross-section is:

$$A_P = 20.3cm^2 \quad (30)$$

3.2.2 LHC kicker generator compensation circuit

According to the description given in 2.3.3 of this document, the compensation circuit natural frequency ω_C will be set by the ripple requirements (12), also (2) links the core cross section and applied voltage-time product. A basic characteristic can be traced assuming same as in principal circuit initial voltage of 39 kV:

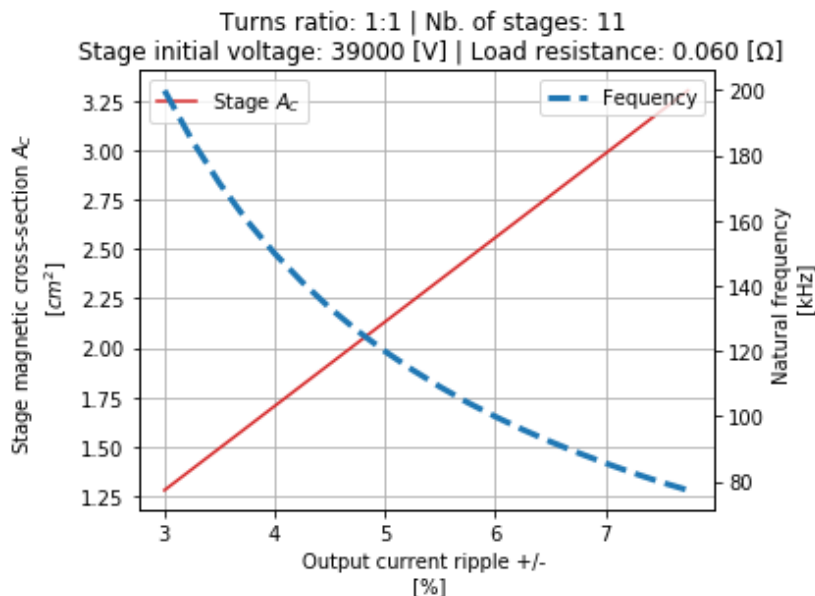


Figure 16: Basic characteristics of the LHC generator compensation circuit in function of d .

It appear, that lower ripple comes along with a smaller core, naturally in this region will require small L_C or big number of primaries N_{PRIM} leading to high switch current over the short period (see figure 6). As a FHCT switch is foreseen for this generator, the number of branches is small, thanks to this the d as low as 5 % is expected (HF ripple 10% see definition figure 6). Resulting requirement for the core cross-section will be:

$$A_C = 2.2cm^2 \quad (31)$$

Once again we'll use the *PythonSymPy* to trace the energy balance (see 2.3.3) in function of cell capacitor C_C , see figure 17.

Obtained value of the capacitor guaranteeing a correct balance in this configuration will be:

$$C_C = 37.2nF \quad (32)$$

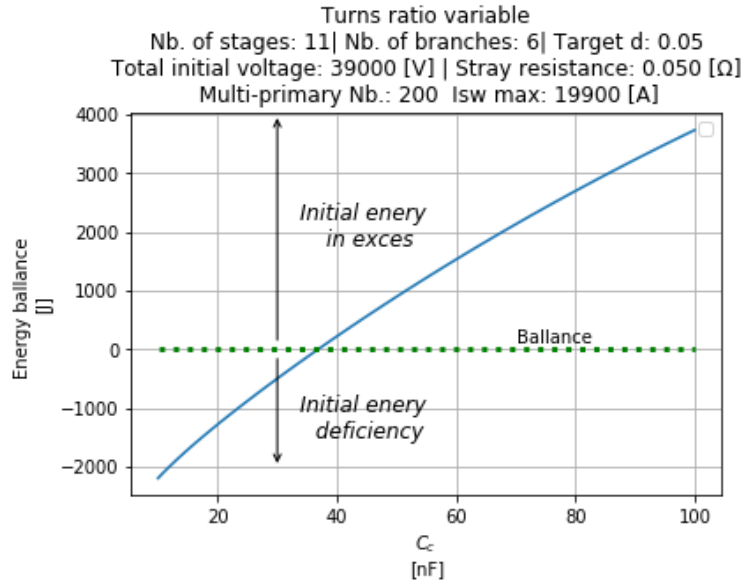


Figure 17: Compensation circuit energy balance.

3.2.3 SPICE Simulation of LHC-like generator

Table 5 lists the parameters slightly adjusted due to differences as in previously.

Table 5: LHC generator SPICE simulation parameters entries.

Parameter	Symbol	Value
Number of branches	N_{br}	6
Number of stages	N_{stg}	11
One stage voltage	V_{init}/N_{stg}	39 kV/ N_{stg}
Principal cell parameters		
Cell capacitor	C_P	36 nF
Cell inductor	L_P	4 μ H
Cell stray resistance	R_σ	50 m Ω
Number primaries	N_{PRIM}	40
Core cross section	A_P	20 cm ²
Compensation cell parameters		
Cell capacitor	C_C	36 nF
Cell inductor	L_C	48.6 μ H
Cell stray resistance	R_σ	50 m Ω
Number primaries	N_{PRIM}	220
Core cross section	A_C	2.2 cm ²

3.2.3.1 LHC generator SPICE simulation of nominal waveform

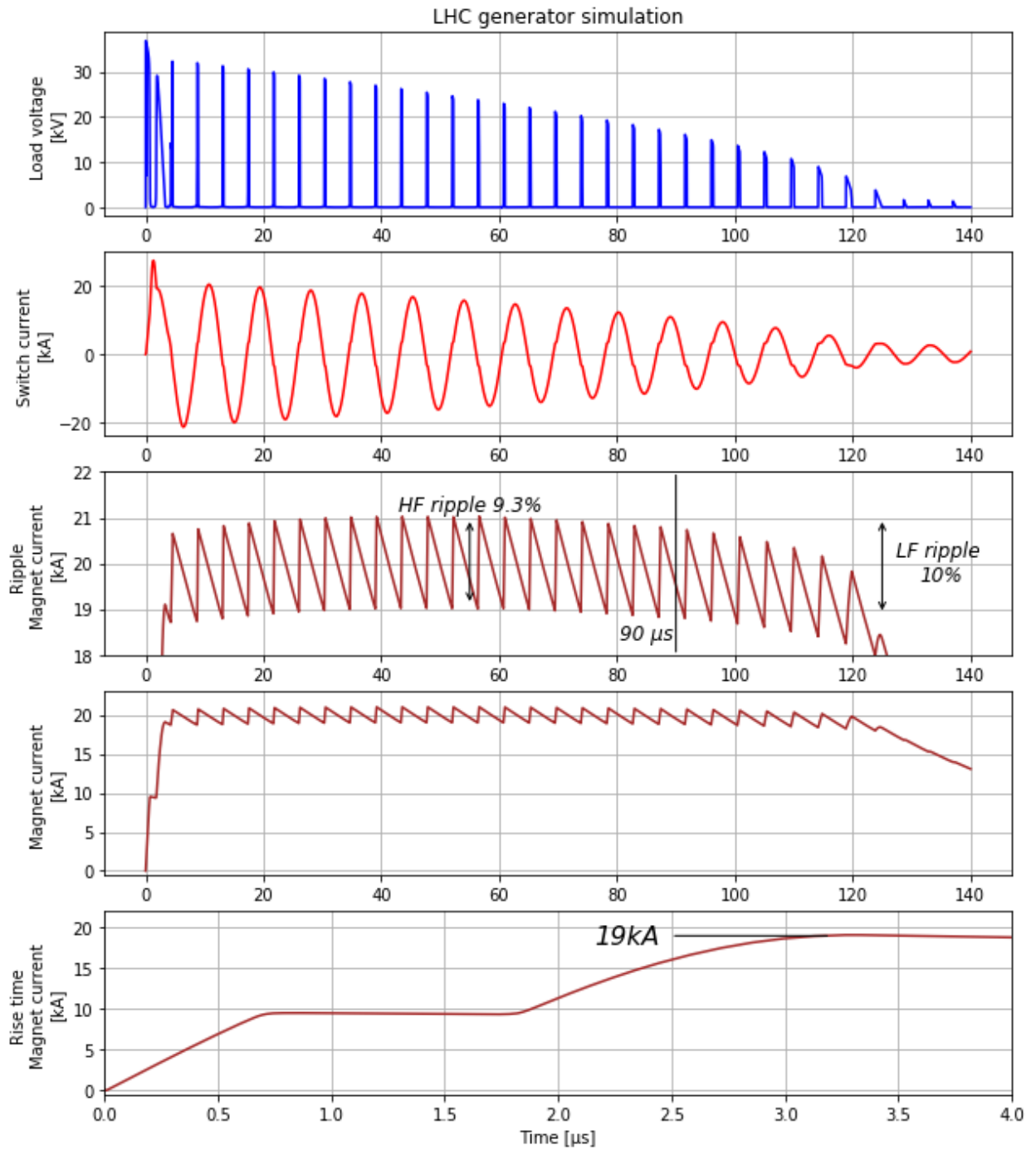


Figure 18: LHC generator simulation of the nominal waveform.

3.2.3.2 LHC generator, basic semiconductor switch considerations

Collected waveforms indicate FHCT as the most suitable technology regarding configuration Tab. 5.

Table 6: LHC generator switch, basic requirements.

Parameter	Symbol	Value
Permanent DC voltage	V_{DC}	$> 3.5 \text{ kV}$
Max. Pulse Current	I_{PULSE}	$> 27 \text{ kA}$
Maximum non-repetitive rise rate	di/dt_{max}	$> 27 \text{ kA}/\mu\text{s}$
Bidirectional	-	Yes

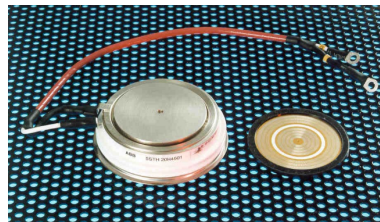


Figure 19: Potentially compatible semiconductor switch from ABB, model 5STH-2045H0002 .

3.2.3.3 LHC generator SPICE simulation of one switch spontaneous trigger

The modular approach will allow to limit the consequences of possible cell spontaneous trigger. Simulation will predict the current and peak energy in the magnet due to this failure mode:

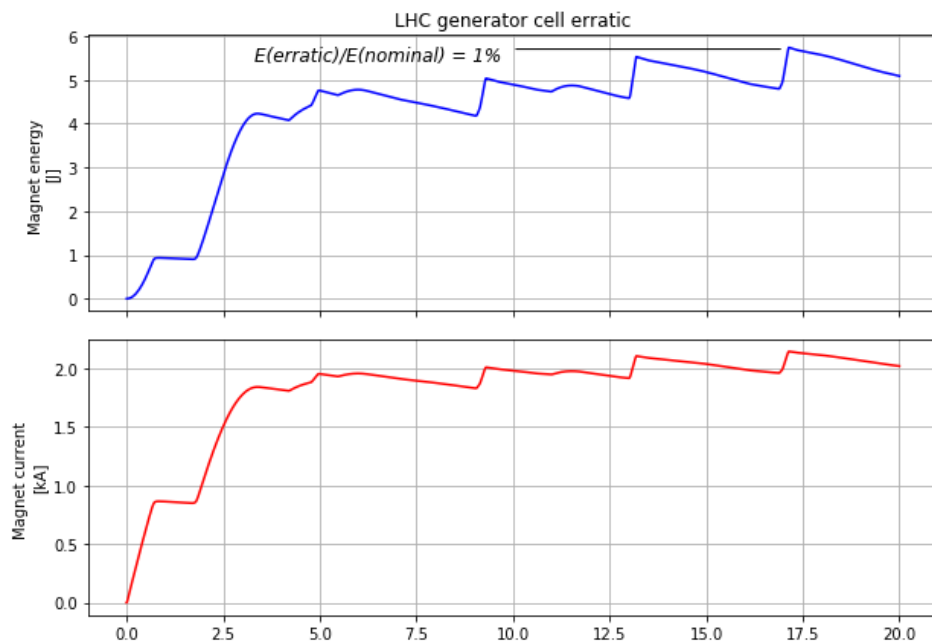


Figure 20: LHC generator simulation, one cell spontaneous trigger.

3.2.4 LHC generator assembly considerations

For the purpose of assembly considerations the nanocrystalline VITROPERM cores with epoxy resin coating were selected. Principal core of each cell could be obtained with 3 stacked sets of L2160-W631 + L2194-V105 cores. Compensation core could be obtained using five L2040-W624 cores. The rectifiers of each branch are not represented in figure 21.

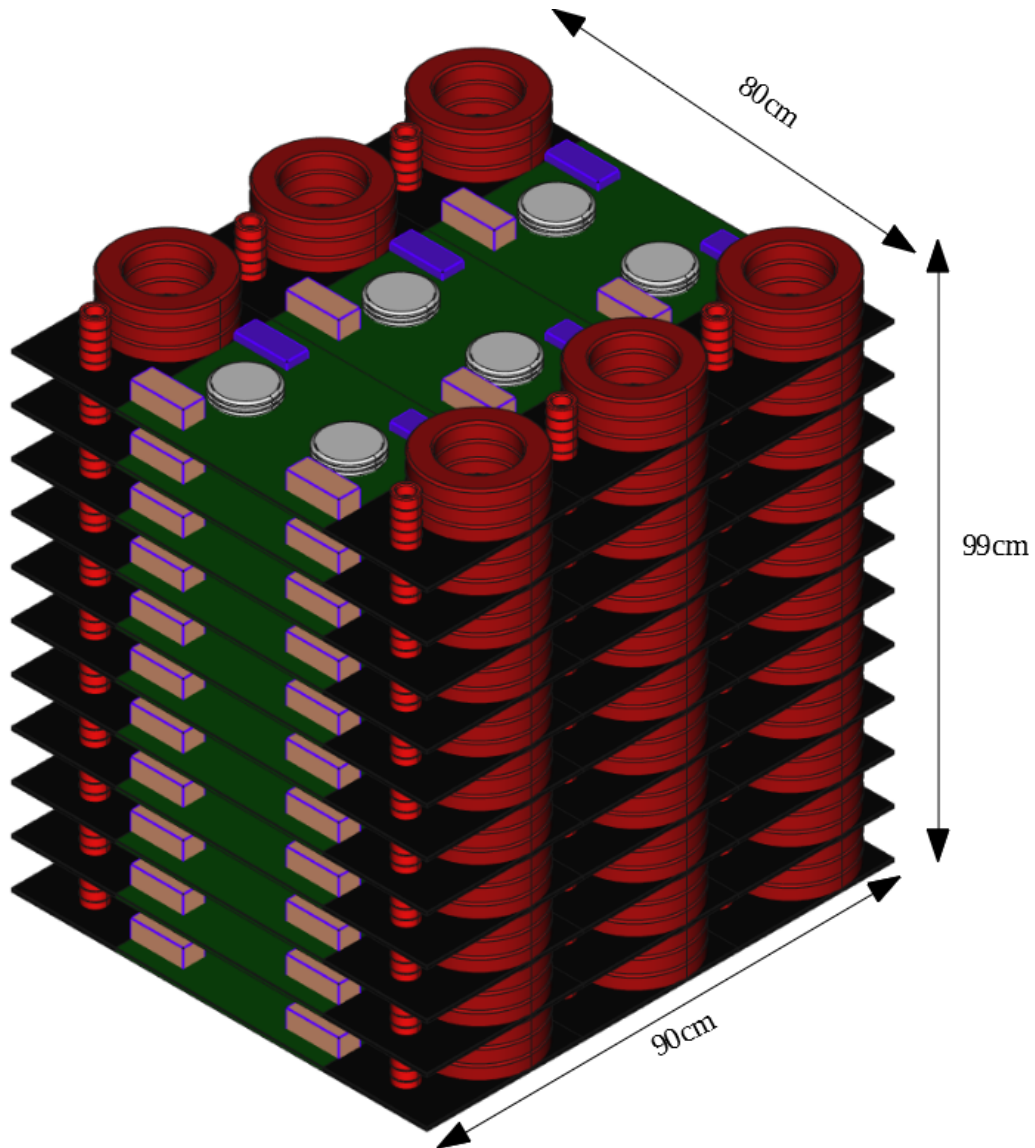


Figure 21: LHC generator assembly view (*FreeCAD*).

4 Conclusions

The study has shown in simulation, the feasibility of example designs based on AC IA topology. Demanding requirement in terms of peak power over the rise time and flattop stability are met.

Performance (flattop stability and rise time) may be easily scalable at the cost of the volume and switches number.

Topology is robust to the short-circuit condition of the load, as the maximal current is defined by the discrete cell energy, initial voltage and the ω of the LC circuit.

Topology will be robust so some catastrophic scenarios, such as radiation levels destroying all switches (short-circuit) of the system at once. Per principle, a correct pulse will be delivered to the load.

The modular approach allows to limit the consequences of possible cell missing/ erratic failures as the energy stored in an individual cell is only 4% and 1% fraction of the nominal magnet energy. This gives an opportunity for a missing/ erratic tolerant system. High voltage (sum of all stages) appears at the output only over the pulse generation, which reduces the sparking probability and an accidental signal coupling to the controls.